



# Insights into the function of ion channels by computational electrophysiology simulations☆

Carsten Kutzner <sup>a,1</sup>, David A. Köpfer <sup>a,1</sup>, Jan-Philipp Machtens <sup>b</sup>, Bert L. de Groot <sup>a</sup>, Chen Song <sup>c</sup>, Ulrich Zachariae <sup>d,e,\*</sup>

<sup>a</sup> Department of Theoretical and Computational Biophysics, Computational Biomolecular Dynamics Group, Max Planck Institute for Biophysical Chemistry, Göttingen, Germany

<sup>b</sup> Institute of Complex Systems, Zelluläre Biophysik (ICS-4), Forschungszentrum Jülich, Jülich, Germany

<sup>c</sup> Department of Biochemistry, University of Oxford, United Kingdom

<sup>d</sup> Physics, School of Science and Engineering, University of Dundee, United Kingdom

<sup>e</sup> Computational Biology, School of Life Sciences, University of Dundee, United Kingdom



## ARTICLE INFO

### Article history:

Received 2 November 2015

Received in revised form 3 February 2016

Accepted 4 February 2016

Available online 10 February 2016

### Keywords:

Molecular dynamics

GROMACS

Electrophysiology

Ion channels

Conductance

Selectivity

## ABSTRACT

Ion channels are of universal importance for all cell types and play key roles in cellular physiology and pathology. Increased insight into their functional mechanisms is crucial to enable drug design on this important class of membrane proteins, and to enhance our understanding of some of the fundamental features of cells. This review presents the concepts behind the recently developed simulation protocol Computational Electrophysiology (CompEL), which facilitates the atomistic simulation of ion channels in action. In addition, the review provides guidelines for its application in conjunction with the molecular dynamics software package GROMACS. We first lay out the rationale for designing CompEL as a method that models the driving force for ion permeation through channels the way it is established in cells, i.e., by electrochemical ion gradients across the membrane. This is followed by an outline of its implementation and a description of key settings and parameters helpful to users wishing to set up and conduct such simulations. In recent years, key mechanistic and biophysical insights have been obtained by employing the CompEL protocol to address a wide range of questions on ion channels and permeation. We summarize these recent findings on membrane proteins, which span a spectrum from highly ion-selective, narrow channels to wide diffusion pores. Finally we discuss the future potential of CompEL in light of its limitations and strengths. This article is part of a Special Issue entitled: Membrane Proteins edited by J.C. Gumbart and Sergei Noskov.

© 2016 Elsevier B.V. All rights reserved.

## 1. Introduction

Ion channels are integral membrane proteins abundant across a vast range of cell types [1]. They facilitate the passive, selective permeation of ions such as sodium, potassium and chloride through the phospholipid bilayer, which is otherwise impermeable for ions [2]. Ion channels fulfill essential functions as diverse as electrical signaling underlying neuronal function and muscular contraction, cell volume regulation, and cellular ionic homeostasis [2,3]. Whole-cell and single-channel electrophysiological experiments provide a wealth of information on channel features such as ion conductance and selectivity. Electrophysiology recordings have established that many ion channels exhibit multiple conducting states and that the gating between these states is a major hallmark of ion channel function [1,4]. As they are omnipresent and fulfill vital

physiological roles, the malfunction of ion channels gives rise to several critical diseases also termed channelopathies [5]. It is therefore essential to understand the mechanisms underlying physiological as well as pathological ion permeation through ion channels and its regulation.

A major breakthrough in this field was achieved by the resolution of atomic structures of ion channels, pioneered by seminal work on potassium channels, more recently followed by chloride channels, sodium channels and calcium channels [6–10]. Prior to these advances, some wider pore non-specific channels had already been structurally characterized by X-ray crystallography [11,12]. Taken together, these structures have highlighted not only the variety of architectures employed to facilitate ion permeation, but also provided detailed insight into the interactions of ions within the pore as well as snapshots of open, closed, activated and inactivated channels, yielding a direct structural link to electrophysiological observations.

Despite the wealth of information gained from structural studies, the core of ion channel function, the actual permeation mechanism of ions across the pore, is an inherently dynamic process and therefore challenging to track with static structural studies such as X-ray crystallography. Molecular dynamics (MD) computer simulations have therefore

☆ This article is part of a Special Issue entitled: Membrane Proteins edited by J.C. Gumbart and Sergei Noskov.

\* Corresponding author at: Physics, School of Science and Engineering, University of Dundee, United Kingdom.

E-mail address: [u.zachariae@dundee.ac.uk](mailto:u.zachariae@dundee.ac.uk) (U. Zachariae).

<sup>1</sup> These authors contributed equally to this work.

been utilized extensively to study mechanisms of ion conductance, selectivity, as well as channel gating [13–16], for a review see Ref. [17]. In such simulations, the channel protein, usually embedded in a model membrane patch, is often modeled atomistically in a physiological buffer environment, which enables following the detailed motions of individual atoms and ions with high spatial and temporal resolutions.

However, there are three main challenges associated with simulating ion currents by MD techniques. First, empirical interaction parameters (force fields) in classical MD simulations are approximations and historically lack the explicit description of electronic polarization effects [18]. Therefore, it is critically important to directly evaluate the accuracy of simulation results, for example by comparison to experimental data. Second, due to the small integration time step and the number of interactions to be evaluated per step, the overall attainable simulation time is limited, currently usually to the microsecond timescale for typical simulation systems on state-of-the-art computer hardware [19]. This restricts the application of atomistic simulations to the investigation of ion currents that are minimally in the pA regime and often precludes the unbiased simulation of gating and permeation events. A third, and partially related, issue is associated with enforced ion translocation. The natural driving forces for permeating ions are a transmembrane voltage and concentration gradients across the membrane. In a normal MD simulation, however, any concentration or charge gradient will quickly dissipate unless external forces are applied or a protocol restoring the gradients.

External electric fields have long been in use for MD simulations of ion transfer [20–24]. With periodic boundary conditions (PBC) and a single-bilayer setup, both sides of the membrane effectively form the same compartment, except that their electrostatic potential differs [25, 26]. Simulations of sustained ionic flow are thus possible at equal ion concentrations on both sides of the membrane. A separating vacuum or air slab has been introduced [27–29], enabling the simulation of single-membrane setups with different concentrations on both sides of the membrane, however in turn preventing sustained ionic flow as ions cannot pass the vacuum slab. Recently, an energy step was introduced in the aqueous compartment that permits different ion concentrations on both sides of a single membrane [30]. Alongside the use of external electric fields, umbrella potentials have widely been utilized to enforce ion displacements and thereby to record the free energy profile of permeation events [31,32]. This powerful method is challenged primarily by the required choice of a reaction coordinate, which is a non-trivial task for multi-ion permeation events or large pores, and therefore often necessitates the acquisition of multidimensional potentials of mean force. For small voltages, conductances can even be predicted from equilibrium simulations, if statistically sufficient spontaneous permeation events can be recorded on the timescales accessible to the simulation [33].

In this contribution, we review the results of an alternative simulation strategy termed Computational Electrophysiology (CompEL) [34], which permits the user to control both concentration gradients and voltage across the membrane. In this method, the driving force for ionic movements is a transmembrane voltage or an ion concentration gradient. As opposed to applying an external electric field, the voltage in CompEL simulations is “internal” in the sense that it results from an ion concentration difference between two aqueous compartments [27, 35,36], similar to the situation in the cell, where Nernst concentration gradients occur across the cell membrane. The separation of two compartments in a periodic simulation system is obtained by duplicating the membrane patch in the direction of the membrane normal. Such an arrangement of two membranes in a periodic system results in an inner and outer compartment, of which the latter is connected across the periodic boundaries (Fig. 1).

By choosing a small ion imbalance  $\Delta q$  between the two compartments, a voltage across both membranes is generated, analogous to the creation of transmembrane voltages in biological membranes. As described in Ref. [28], this transmembrane voltage is due to the

capacitance  $C$  of the membrane, which behaves as a capacitor separating the compartments, and the voltage  $\Delta U$  is related to the charge imbalance through the equation  $\Delta U = \Delta q / C$ . Because the capacitance of the bilayer is relatively small (on the order of  $\sim 1 \mu\text{F cm}^{-2}$  [27,28,35, 37]), an imbalance of a few ions is often sufficient to evoke a considerable voltage across the membrane in a small atomistic simulation system. However, the desired voltage can be further adjusted by slightly adapting the area of the lipid patch used in the simulations, so that physiological voltage levels are usually easily obtained.

Under normal conditions, this voltage would soon be depleted by ion translocation events through a membrane channel. However, by continuously monitoring the ion counts in the two aqueous compartments during the simulation, CompEL can maintain any desired imbalance by performing ion/water position exchanges between the compartments as needed (Fig. 3). In a similar way, independent bulk ion concentrations can be imposed on either side of the membrane. This, for example, allows the simulation of channel reversal potentials. CompEL thus enables simulations at a sustained transmembrane voltage or under a constant transmembrane ion concentration gradient. Observables that can be derived from a CompEL simulation include ionic conductances, selectivities, and pathways, as well as current–voltage (I–V) curves and the possible rectification behavior of the channel under consideration.

Our review is structured as follows. We begin with a detailed description of the simulation protocol, including a practical guide for the setup and execution of CompEL simulations. We then present five recent examples in which CompEL simulations have yielded new insights into the functional mechanisms of ion channels and pores. These include the wide beta-barrel channels PorB and VDAC, the channel-forming assembly of dermcidin, the potassium channel KcsA, and the anion channel that is intrinsic to secondary active glutamate transporters (EAATs). We conclude this review with a discussion of the limitations and strengths of CompEL and final remarks.

## 2. The CompEL setup: principles and application

When aiming to replicate the characteristic behavior of a protein in a molecular simulation, it is ideally placed in an environment that closely mimics its natural habitat. Therefore, membrane channels are embedded in lipid bilayers and solvated by water and ions, while PBC are used to eliminate surface artifacts. For a CompEL setup [34], two copies of such a channel/membrane system are stacked vertically, and thus PBC form two separated aqueous compartments (blue and gray in Fig. 1A, B). Under physiological conditions the lipid bilayer is virtually impermeable to water molecules and ions, which therefore need to pass through a channel to travel from one compartment to the other.

The most commonly used, ‘deterministic’, protocol [34] of CompEL sets reference counts for the number of positive and negative ions in each compartment. If at any time the actual number of ions differs from the reference count, ions from one compartment are swapped with water molecules from the other compartment until the reference counts are restored. This way, a gradient in ion concentration and/or electric charge between the compartments can be set and maintained over time against dissipation by ionic channel currents. The resulting steady state permits recording the flux of ions through each channel over time similar to single-channel electrophysiology measurements. The electric potential difference  $\Delta U$  (Fig. 1D) is a direct result of the imposed charge imbalance  $\Delta q$ . In CompEL convention, each ion with charge  $\pm e$  removed from one and added to the other compartment changes  $\Delta q$  by  $\pm 2e$ ; however the total charge of the system remains unchanged. The total charge of a periodic simulation system should be zero when long-range electrostatics are treated with the Particle Mesh Ewald (PME) method, as a net total charge can lead to artifacts, especially for membrane systems [39]. To minimize the impact of the ion/water positional exchanges (see Fig. 5 in Ref. [34]), only particles that fulfill a maximum distance criterion to the compartment boundaries (and

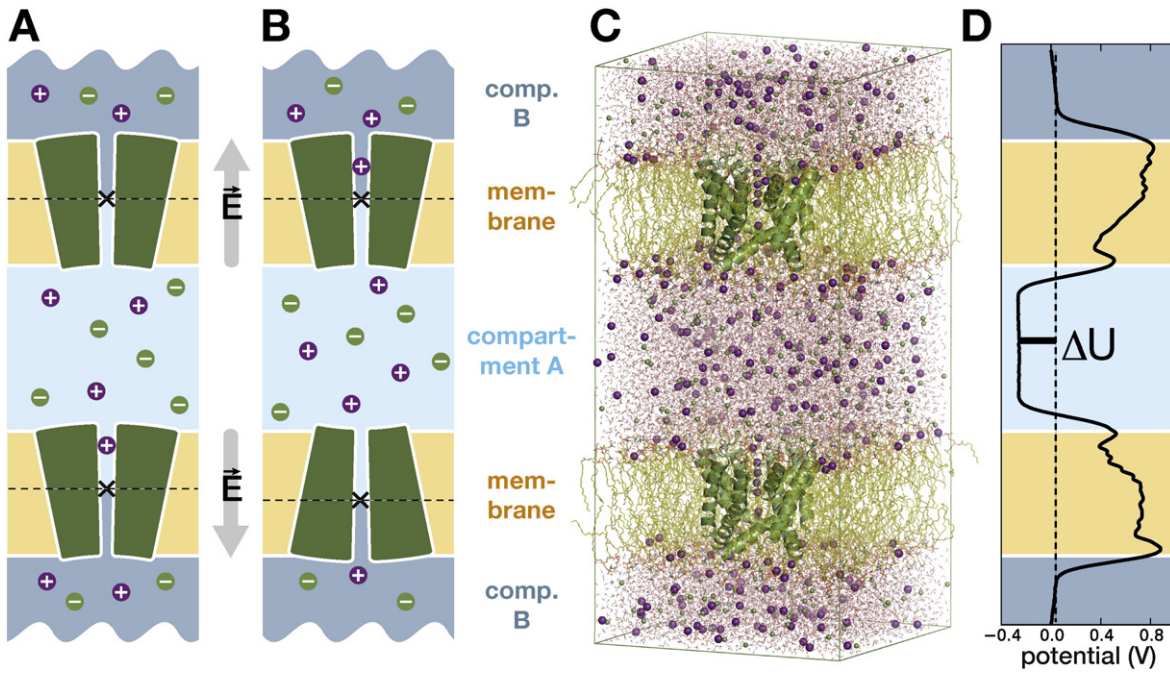


**Fig. 1.** Computational Electrophysiology (CompEL) setup encompassing two lipid membranes. (A, B) Schematic of the simulation system including the two membranes (yellow), two protein channels (green), water (blue/gray), anions (green  $-$ ), and cations (purple  $+$ ). In case of parallel channel alignment (A), one channel experiences an inward, the other an outward directed electric field  $\vec{E}$  (gray arrow). For an antiparallel orientation (B), both channels experience the same field direction. Panel (C) shows the parallel KcsA setup used in Ref. [38] and (D) the average potential along  $z$  resulting from a  $\Delta q = 2e^-$  charge imbalance, where  $\Delta U$  denotes the potential difference between the compartments. (Panel C appeared as Fig. 1C of Ref. [38].)

thus to the channels and membranes) are selected for the exchange. As a result, any discontinuity arising in the atomic forces for atoms near the membrane is negligibly small, as demonstrated for ions traversing a KcsA potassium channel in Fig. 2.

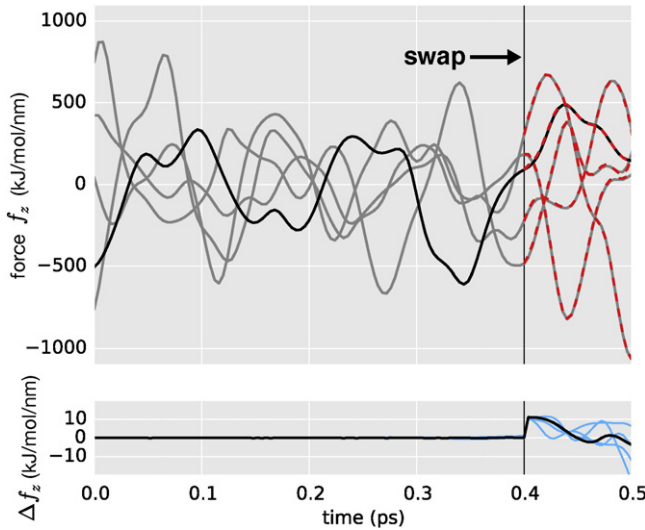


**Fig. 2.** A distant ion/water position exchange has a negligible effect on the ions in the channel. For five  $K^+$  ions within the KcsA channel described in Section 3.2 [38], atomic forces are shown for a representative time interval of 0.5 ps length (top panel). Gray lines show the  $z$  component (along the pore axis) of the force  $f_i$  for  $i = 1, \dots, 5$  on each ion for a reference simulation without any ion/water position exchange. The dashed red lines show the same forces for a case where at  $t = 0.4$  ps a water molecule is exchanged with an ion. The impact on the forces experienced by the  $K^+$  ions is almost unnoticeable in the time-series, as the forces change by just a few percent as a response to the exchange. The lower panel shows the difference  $\Delta f_z$  between the observed forces with and without exchange. Note that  $\Delta f_z$  is about three orders of magnitude smaller than the typical fluctuations in  $f_z$ . The black lines in both panels highlight  $f_z$  and  $\Delta f_z$  for one of the five  $K^+$  ions.

One might think that CompEL, due to the doubled system size, has a high computational overhead. However, the sampling efficiency in fact remains unchanged, because ion permeation events are recorded simultaneously across two channels, and thus about twice as many permeation events occur per simulation time. One might also argue that a small computational disadvantage remains because PME does not scale linearly with particle number  $N$ , but instead follows an  $N \log(N)$  relationship. This however applies only to a small part of the total calculations, namely the fast Fourier transformation (FFT), which expends about 10% of the total time of a typical GROMACS time step. By contrast, most of the computational time is spent in operations that scale linearly with  $N$ , such as the short-range part of the Coulomb and van der Waals forces, bonded interactions, and other PME work which includes spreading the charges on the FFT grid or extrapolating the long-range forces from the grid.

To quantify the small impact of the increased system size on sampling efficiency, we performed benchmarks on a workstation with an Intel E5-1620 CPU (3.60 GHz) and an NVIDIA GTX 680 GPU using GROMACS 5.0. We used two different MD test systems comprised of 58,975 and 195,051 particles, respectively, for each single-membrane system. A time step of 4 fs, PME electrostatics, and cutoffs of 1.2 nm were employed. In the case of the smaller box, the average performance over four runs was 50.98 ns/day (single-layered) and 23.52 ns/day (double-layered), corresponding to a reduction of ~8% in sampling efficiency for the double system. Simulating the larger box, we obtained 7.82 ns/day for the single-layered membrane and 3.98 ns/day for the double-layered system. This translates into an increase of ~1% in sampling efficiency for the double system.

## 2.1. Setting up CompEL simulations with GROMACS

GROMACS [40] versions 5.0 and later have built-in support for CompEL simulations [41]. MD systems consisting of a membrane-embedded channel in a water box are easily adapted for CompEL by stacking two copies of the system on top of each other, for instance by using `gmx genconf-nbox 1 1 2`. This yields a double-layered system with a

parallel alignment of the two channels (Fig. 1A). In this case, the stacking merely doubles the size of the periodic unit cell in z dimension, so when starting from a well-equilibrated single-layered system, no further equilibration is needed. In order not to introduce gaps in molecules crossing box boundaries, all molecules need to be made whole before changing the periodic representation, for example by using gmx trjconv -pbc mol. Differences in ion counts between the compartments result in a potential gradient that is positive across one channel or membrane and negative across the other with respect to channel orientation. This setup can directly uncover possible rectification effects, in addition to ionic conductances and selectivities. If instead maximum sampling for either an inward or an outward gradient across the channel is desired (e.g., only under positive or negative voltages), the MD systems can be stacked upside down on top of each other (Fig. 1B), so that both channels experience the same gradient. The supplementary information (SI) contains a bash script that prepares a CompEL setup from a single-layered MD system.

CompEL is activated by changing the GROMACS .mdp input file entry swapcoords = no to swapcoords = Z (for systems that are stacked in the z direction). Typical CompEL parameters including example values are given in Table 1. Alternatively, they can be retrieved from the mdout.mdp file produced by running gmx grompp on an .mdp file that includes the line swapcoords = Z. The swap-frequency parameter controls the number of MD steps after which the protocol periodically checks for potential mismatches between the set ion counts and determines whether exchanges are necessary. The .mdp file expects several names of index groups to define the ions, the solvent, and the channels. The -twin switch of gmx make\_ndx constructs index groups for the double-layered system from the index file of the single-layered system.

A crucial parameter is the choice of the group of atoms (split-group0 and 1) that define the compartment boundaries in z (dashed lines in Fig. 1A, B) by their, optionally mass-weighted, center (× in the figure), depending on the value of massw-split. These groups of atoms will usually be part of the channels themselves, ideally chosen such that each of their centers coincides with the midplane of the lipid membrane the channel is embedded in. This is important because the

ions will be assigned to the A and B compartments based on these two geometrically defined planes.

The group of water molecules that can be exchanged with ions is defined by the index group solvent-group. For ions under the control of the CompEL swap protocol, GROMACS 5.0 and 5.1 expect a single index group swap-group, containing both the positive and negative ionic species grouped together. Here, reference numbers for the ions are set with the anions and cations parameters per compartment, which essentially determine the charge and/or concentration imbalance to be sustained. Later versions allow the user to control a variable number iotypes of ionic species. For each type, the name iotype0-name as well as reference counts iotype0-in-A, iotype0-in-B must be provided. Ions may in principle also consist of more than a single atom, provided they are still small enough to be exchangeable with a single water molecule.

For coupl-steps > 1, time-averaged rather than instantaneous ion counts determine whether exchanges are performed, which can reduce unnecessary back-and-forth exchanges. For situations where the positional exchanges should not occur near the middle of the compartments, for instance in cases where a protein extends farther into a compartment, the bulk-offset parameter defines which regions are acceptable for the exchanges (Fig. 3). See also the CompEL section of the GROMACS manual [42] for additional details.

## 2.2. Analyzing CompEL results: determining ion flows and voltages

The potential difference  $\Delta U$  resulting from a particular charge imbalance  $\Delta q$  can be calculated from the atomic positions (charges) stored in the .xtc trajectory file, for instance by using gmx potential (see Fig. 1D for an example). For a low-noise potential curve  $\Delta U(z)$ , a sufficient number of individual snapshots (i.e., trajectory frames) should enter the time average; see also the section on ‘voltage fluctuations in small systems’ in Section 4.

The output file swapions.xvg produced by CompEL records the number of ions in each compartment at each CompEL step, the differences to the requested counts, the performed number of positional exchanges, and each permeation event across the channels. Provided that ions cannot pass through the membrane, which for instance might occur in insufficiently equilibrated systems, the number of channel permeations on average equals the number of ion/water position exchanges. The average current  $I$  (charge transfer per time), summed up over both channels, can therefore be directly calculated from the recorded number of ion/water position exchanges and the charge of the exchanged ions. The average conductance  $G$  of a single channel (adding the factor 0.5) can be calculated from the ionic current and the potential difference as  $G = 0.5 I / \Delta U$ , see the Section ‘Calculation of ion selectivity and conductance’ in Ref. [34]. The simple number of exchanges does however not permit any discrimination between the two channels, which would be required, for example, to quantify rectification effects occurring in a parallel channel setup (Fig. 1A). Therefore, CompEL has a built-in mechanism that counts permeation events per channel and ion type. To enable this, two virtual cylinders are defined around the channels such that when an ion travels from one compartment to the other across a channel it will also traverse one of the virtual cylinders (Fig. 4). Each cylinder is defined relative to the center of its associated channel and should be large enough to encompass the channel pore. Ions traveling through the channel from compartment A to B are counted as positive and those traveling from B to A as negative flux. For an ion to be counted as having passed a channel, it needs to be recorded in one compartment at some time  $t_{\text{before}}$ , then at  $t_{\text{chan}} > t_{\text{before}}$  within the cylinder, and finally at  $t_{\text{after}} > t_{\text{chan}}$  in the other compartment. If the cylinder is very thin in z direction and the time interval between CompEL steps is long, ions might pass the channel without ever being detected inside them. To prevent this, the cylinders can either be expanded and/or the frequency of CompEL steps increased.

**Table 1**  
Input parameters controlling CompEL simulations.

```
; Swap positions along direction: no, X, Y, Z
swapcoords      = Z
; Swap attempt frequency
swap-frequency   = 100
; The center of the following two index groups will define the
; compartment boundaries
split-group0     = channel0
split-group1     = channel1
; Use the mass-weighted center of the split groups (yes/no)
massw-split0     = no
massw-split1     = no
; Name of solvent molecules
solvent_group     = SOL
; Average the number of ions per compartment
; over these many swap attempt steps
coupl-steps       = 10
; Number of ion types to be controlled
iotypes          = 3
; Names of the ion types that can be exchanged with solvent molecules
iotype0-name      = NA
iotype0-in-A      = 51 ; requested number of NA ions in comp. A
iotype0-in-B      = 35 ; req. number of NA ions in B
iotype1-name      = K
iotype1-in-A      = 10 ; req. number of K ions in A
iotype1-in-B      = 38 ; req. number of K ions in B
iotype2-name      = CL
iotype2-in-A      = -1 ; -1 means: use the number of ions
iotype2-in-B      = -1 ;           as found at time step 0
; Offset compartment-defining layers
bulk-offsetA      = 0.0
bulk-offsetB      = 0.0
; Split cylinder dimensions (nm), for counting ion permeations
cy10-r           = 2.0
cy10-up          = 1.0
cy10-down        = 1.0
cy11-r           = 2.0
cy11-up          = 1.0
cy11-down        = 1.0
```

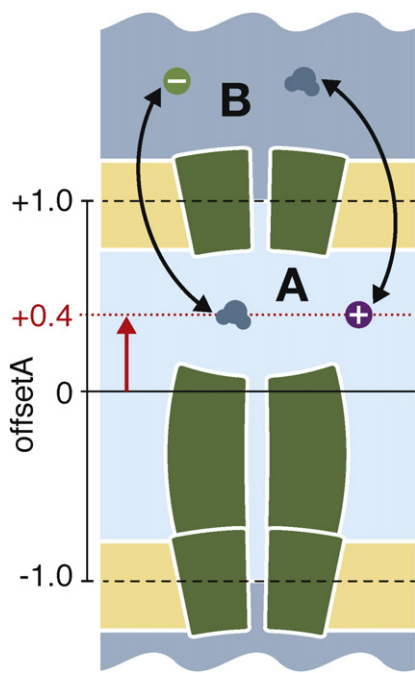


**Fig. 3.** Definition of the bulk-offset parameter. If the channel extends far into one of the compartments, an offset  $b$  ( $-1 < b < +1$ , red dotted line) can be defined to ensure that ion/water position exchanges occur in the bulk liquid instead of near the channel protein.

As the history of the ions at  $t_{\text{before}}$  is not known at the start of a simulation, ions located within the cylinders at startup cannot be counted as permeation events until they first leave the channel. Therefore, it may take a few nanoseconds until the number of permeation events per time interval is reliably recorded. It is important to note that the selected dimensions of the cylinders have no influence on the positional exchanges or the CompEL protocol in general, as they merely provide an on-the-fly count of ion flux per channel and ion type.

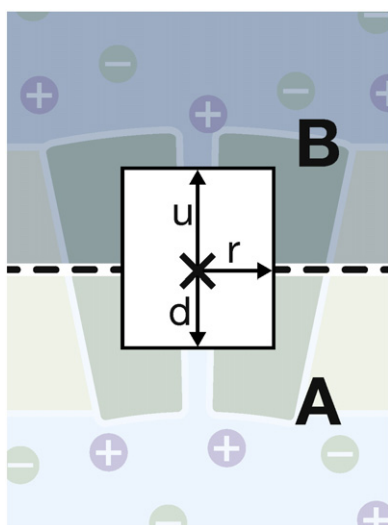


**Fig. 4.** A virtual cylinder (white) can optionally be specified to record the specific channel and direction of each ion permeation event. The imaginary cylinder is defined relative to the center ( $x$ ) of the channel, with a radius  $r$ , and upward and downward extensions  $u$  and  $d$ . The black dashed line denotes the – independently defined – compartment boundary that separates compartment A from B.

### 3. Results obtained by application of CompEL

#### 3.1. Antibiotic resistance variants of the bacterial porin PorB and gating of the mitochondrial porin VDAC

Porins were the first membrane channel proteins to be crystallized and structurally determined by X-ray diffraction [11,12,43]. They were also among the first integral membrane channels in which ion permeation was studied by atomistic MD simulations [21,44,45]. Most porins form wide beta-barrel pores that occur in the outer membrane of Gram-negative bacteria, mitochondria and chloroplasts [46]. In Gram-negative bacteria, they mediate the largely unspecific diffusion of hydrophilic molecules such as nutrients, ions and water across the low-permeability outer membrane. In mitochondria, porins are the major gates for exchange of ATP and ADP with the cytoplasm, and are also thought to be involved in apoptotic pathways [47].

Recently, bacterial porins have attracted renewed interest as they not only provide inward diffusion pathways for nutrients, but also for antibiotic molecules, which often contain charged or polar chemical moieties. Indeed, in Gram-negative bacteria, influx through porins is the major entry mechanism for common antibiotics [48]. It has been shown that mutations in the beta-barrels therefore play a role in the development of antibiotic resistance in pathogens [49].

PorB is the major porin in the outer membrane of the two pathogenic Gram-negative organisms *Neisseria meningitidis* and *Neisseria gonorrhoeae* [50]. It plays decisive roles in the infection of hosts and the development of their immune response [51]. Single-point mutations have been detected in PorB variants of resistant strains, which contribute to their diminished antibiotic susceptibility. These mutations usually affect the central pore, most often the eyelet region, such as the mutation G120K in *N. gonorrhoeae* PorB or the homologous substitution G103K in *N. meningitidis* PorB [50,52].

In the first set of CompEL studies, the pathways taken by anions and cations through PorB were investigated [34]. Due to its wide channel cross-section, Neisserial PorB has a large single trimer conductance of about 1.0 nS at 200 mM KCl, which enabled the recording of a vast number of ion permeation events. After ensuring that the conductance predicted by CompEL was in very good agreement with experiments [52], it became clear that, although the pore remains wide along most of the channel axis, single-point mutations in the eyelet region can have a marked influence on its permeability for different ion types. In wild-type *N. meningitidis* PorB, for instance, a clear separation of the permeating ions into a wide pathway for anions and one for cations was seen (Fig. 5, left). By contrast, the mutation G103K leads to a nearly complete disruption of the cationic pathway in the pore center, while the route for anions is almost unaffected (Fig. 5, right) [34].

The anticipated impact of such a perturbation on antibiotic influx is substantial, because most traditional antibiotics incorporate highly polar chemical moieties, and polar antibiotics preferentially enter the bacterial cell across porins [48,49]. While wild-type PorB would be able to complement both positive and negative partial charges in an antibiotic molecule as it travels through its central eyelet, the mutant would present a higher barrier to the positive face of a molecule, which would likely result in a lower overall translocation rate and the need for reorientation.

It is important to note, however, that despite their beta-barrel structure, porins are not simply inert, wide channels allowing the energy-independent exchange of polar molecules across membranes. In most cases, they actually display voltage-dependent gating, an effect that is generally not well understood in porins [53–55]. For some porins, pressure-induced effects on gating have also been reported [56]. One of the most biomedically relevant gating processes of a beta-barrel porin is the voltage-induced closure of the anion-selective channel VDAC, which is located in the mitochondrial outer membrane of eukaryotes [57]. The gating of VDAC is implicated in apoptotic pathways, and can be influenced by apoptotic and antiapoptotic proteins [58]. The structural determinants

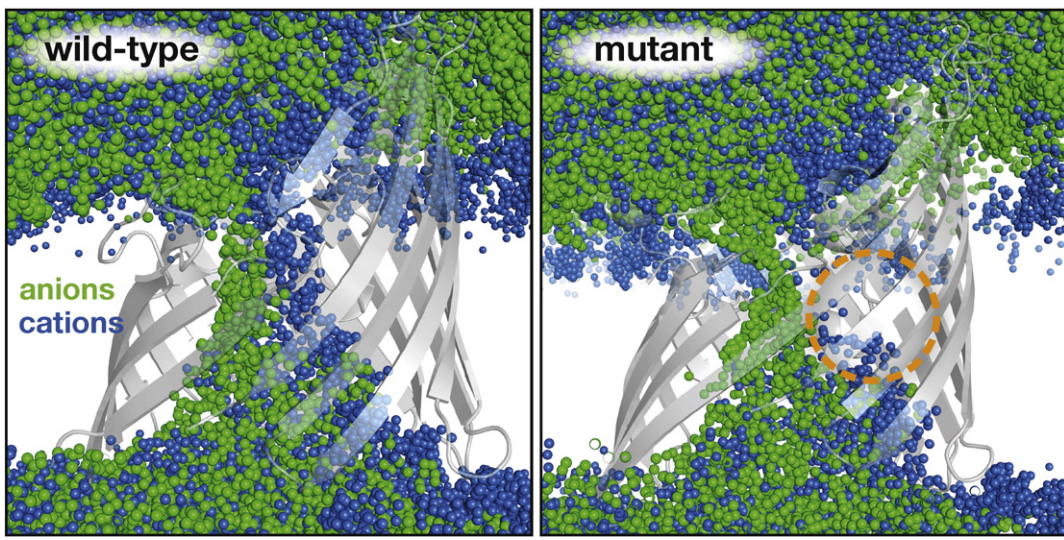


**Fig. 5.** CompEL simulations of the PorB porin show well-separated pathways for anions (green) and cations (blue). Shown are 500 snapshots of ion positions from a trajectory of 100-ns length of wild-type PorB (left) and the G103K mutant. The mutation leads to a disrupted cation pathway (right, orange circle). This plot uses the same data as Fig. 4A and C in Ref. [34].

of voltage-induced VDAC closure, however, have remained enigmatic for decades after its first discovery by electrophysiological recordings. Usually, the observation of gating in porins is attributed to the flexibility of extended extracellular loops, which may be able to dynamically relocate into the barrel and obstruct the permeation pathway [55].

In a joint study comprising results from solid-state NMR, planar lipid bilayer electrophysiology and CompEL simulations, it could be shown that extensive conformational changes of the barrel itself were able to explain the observed combination of VDAC subconductance levels with a major change in ionic selectivity [59]. Under applied pressure, the beta-barrel underwent transitions towards elliptic, semi-collapsed states, which were facilitated by the absence or removal of the N-terminal helix, which is normally located inside the pore [59].

This gating model implies a departure from the commonly held view that beta-barrels are highly rigid structural scaffolds, in which the motion of loops can be the only determinant for changes in conductance levels. This would explain the nearly universal observation of gating in beta-barrel pores [53]. A number of experimental studies on beta-barrels have followed since the first observation of voltage gating, some of which have indeed reported gating and conductance changes in structures in which most or all extended flexible structural elements were affixed to the barrel or deleted [60–62]. These observations lend support to the notion that the barrels themselves exhibit functional dynamics. More experiments are needed, however, to conclusively answer this question.

### 3.2. Insights into the permeation mechanism of $K^+$ channels

Potassium ( $K^+$ ) channels are ubiquitous in all organisms and many of their crucial functions, such as maintaining the resting potential of cells and terminating the action potential in excitable tissue, have been widely investigated [1].  $K^+$  channels form the largest group of ion channels. They assemble into homotetramers and share at their core a highly conserved selectivity filter (SF) motif of six amino acids that form a narrow passage towards the extracellular mouth of the pore [6] (Fig. 7). Much of the interest in  $K^+$  channels can be attributed to the fact that this structural element is highly selective against the smaller of the physiologically most relevant cations,  $Na^+$ , while conducting the larger  $K^+$  cations with rates close to their diffusion limit [63,64]. A wide variety of permeation and selectivity mechanisms have been proposed since the early days of modern electrophysiology to explain this seemingly counterintuitive observation. However, even almost two decades after the first crystal structure of a  $K^+$  channel

was determined [6], the molecular underpinnings of ion selectivity and conduction efficiency remain under debate.

In a recent CompEL study investigating the dynamics of  $K^+$  channels under near-physiological transmembrane potentials, more than 1300 individual  $K^+$  permeation events were recorded and their permeation pathway and mechanism was analyzed [38]. Without making any modifications to the force-fields—common practice in a number of previous studies of ions in the SF—ionic currents through the prokaryotic KcsA (Fig. 6), the eubacterial MthK and the mammalian Kv1.2 channels were observed to be in good agreement with experiments [65].

A closer look at the permeation events through KcsA (Fig. 7) revealed that ions passed the SF by occupying neighboring ion binding sites, and thereby formed direct ion-ion contacts. In fact, the most frequently observed conformation for KcsA showed the two neighboring sites  $S_2$  and  $S_3$  simultaneously occupied. Actual progression of ions through the SF commences after a newly arriving ion from the cavity displaces water molecules that can be present at the intracellular entrance of the SF, and eventually binds to  $S_4$ . Upon binding, the centrally bound ions at  $S_2$  and  $S_3$  are pushed forward to  $S_2$  and  $S_1$ . This configuration quickly relaxes when the ion nearest the extracellular region is expelled from the SF and the incoming ion advances to  $S_3$ ; a rearrangement that completes the cycle. Essentially, an ion pair at  $S_2$  and  $S_3$  is necessary in order to enable high-efficiency conduction upon arrival of an incoming  $K^+$  ion from the intracellular side.

To validate the computational findings in the light of experimental data, recent advances in crystal analysis software [66,67] were used to re-evaluate the ion occupancy in the SF from the deposited diffraction data of several  $K^+$  channel crystal structures. The re-analysis revealed  $K^+$  occupancies close to 1.0 for all binding sites in all investigated  $K^+$  channels. As a consequence, it appears that states with direct ionic contacts at adjacent binding sites are the most frequently visited configurations in the crystals. Notably, the conductive configurations found in the simulations relaxed into the configurations seen in the crystals under the absence of membrane voltage and crystallographic temperature conditions. In addition, it was found that the central ion pair at SF binding sites  $S_2$  and  $S_3$  is occupied over a very wide range of  $K^+$  concentrations, explaining the relative invariance of ion conduction efficiency upon  $K^+$  concentration changes, which has been observed in experiments [7,38].

### 3.3. Ion permeation mechanism of an antimicrobial peptide channel

Antimicrobial peptides, alternatively termed ‘host defense peptides’, are employed by a wide range of organisms including animals and

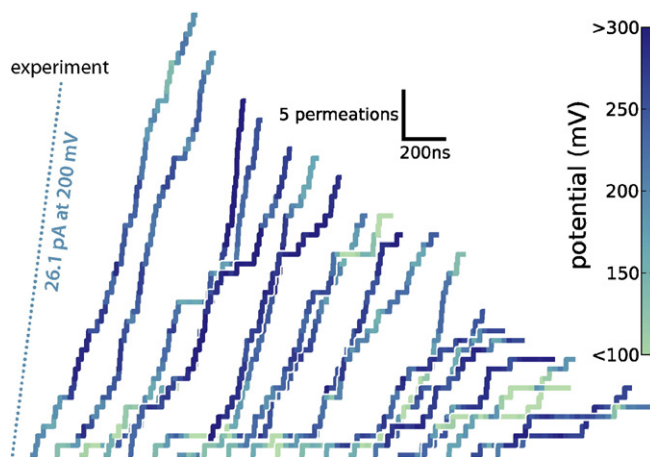


**Fig. 6.** Ionic currents recorded during CompEL simulations of KcsA. Shown are the  $K^+$  permeations in 20 simulations of KcsA under transmembrane potential with channels in the open, conductive conformation and at 400 mM KCl salt concentration (using the same data as Fig. 1D in Ref. [38]). Each upward step in the curves corresponds to one individual ion permeation event. For comparison, the experimentally measured current (data from Ref. [65]) is also shown (dotted).

plants to fight off harmful microbes. These peptides are considered to be a potential basis of a new generation of antibiotics, because they have a substantially diminished risk to cause antimicrobial resistance compared to traditional small-molecule antibiotics [68]. In addition, they often show activity against so-called ‘superbugs’, strains of bacteria resistant to a wide range of customary antibiotics. It is therefore of great importance to understand the functional mechanisms of antimicrobial peptides in action.

Dermcidin is an antimicrobial peptide expressed mainly on human skin and in sweat, which exhibits a broad-spectrum antimicrobial activity. Its oligomeric structure has been resolved by X-ray crystallography [69]. Dermcidin forms a channel-like hexamer composed of three dimers, each of which consists of two anti-parallel  $\alpha$ -helices (Fig. 8A). The static channel structure exhibits a hydrophilic interior, and therefore it had been anticipated that dermcidin might form a water-filled pore. However, due to the narrow constriction sites at both channel termini, it was difficult to ascertain from the crystal structure alone whether the channel actually allows permeation of water and ions through a membrane [69]. Since pore formation and ion conduction has been proposed as a possible functional mechanism of antimicrobial peptides, the dermcidin hexamer was investigated by CompEL to determine its potential ion and water permeability and permeation mechanism.

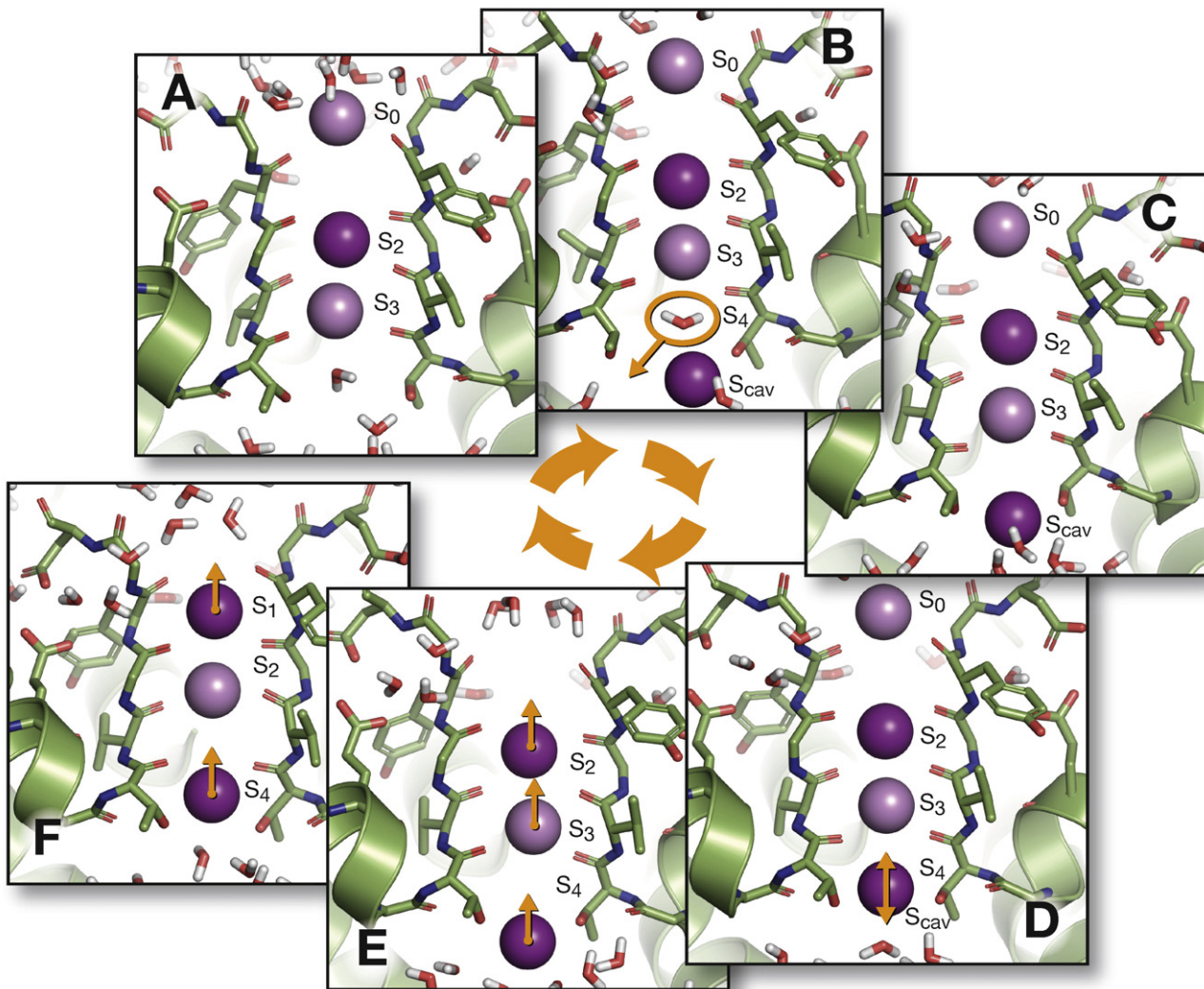


**Fig. 7.** Ion permeation mechanism in the KcsA potassium channel revealed by CompEL simulations. (A) Most frequently found ion configuration in the selectivity filter (SF) with ions tightly bound to S<sub>2</sub> and S<sub>3</sub> and a loosely bound ion at S<sub>0</sub>. (B) An arriving ion at S<sub>cav</sub> from the cavity first displaces a water molecule that can be bound to S<sub>4</sub> (C) before it can access the SF. (D) The arriving ion fluctuates between S<sub>cav</sub> and S<sub>4</sub>, before, in a fast concerted motion, (E) the centrally bound ions are pushed towards the extracellular side, (F) where they bind to S<sub>1</sub> and S<sub>2</sub> before the initial configuration is recovered. (This plot shows the structural configurations previously displayed by Fig. 1E–J in Ref. [38].)

Interestingly, although the channel was initially placed parallel to the membrane normal, it tilted by  $>30^\circ$  with respect to the membrane normal during the equilibration phase of 200 ns (Fig. 8B). This movement was attributed to the reduction of hydrophobic mismatch between the channel exterior and the lipid bilayer.

Ionic reference counts were then set to values that resulted in a transmembrane potential of  $\approx 450$  mV. Compared to physiological conditions, a raised voltage can enable the recording of a greater number of permeation events within the restricted simulation time. The observed ionic currents (Fig. 8C) show that the channel is permeable to both anions and cations, but has a preference for anions. The overall conductance of 108 pS at 1 M NaCl (Fig. 8D) is in good agreement with electrophysiological experiments (81 pS) [69], suggesting that the mechanism of pore formation and ion conduction seen in the simulations reflects the experimental observations and is a likely candidate for the functional mechanism of dermcidin.

Notably, the ions do not permeate along a canonical pathway, i.e., from one channel terminus to the other along the channel axis. Instead, the major permeation pathway displays a zigzag shape: the ions enter the channel at a small opening within the side wall, then move along the channel axis to the opposite side, and exit at another gate within the side wall (Fig. 8B). Arguably, this unique and unexpected pathway would have been difficult to identify with equilibrium MD simulations or potential of mean force calculations.

#### 3.4. Identification of the $\text{Cl}^-$ channel within secondary active glutamate transporters

Glutamate is the major excitatory neurotransmitter in the human central nervous system. Excitatory amino acid transporters (EAATs) terminate glutamatergic signaling by pumping the released transmitter back from the synaptic cleft into nearby neurons and glial cells. EAATs are secondary active transporters, i.e., glutamate uptake is coupled to the co-transport of three  $\text{Na}^+$  and one  $\text{H}^+$  in exchange for one  $\text{K}^+$  ion [70]. Interestingly, EAATs also operate as anion-selective channels

[71]. The EAAT anion conductance is assumed to regulate neuronal excitability and signal transmission [72], and an impairment can be associated with neurological disorders [73].

Several crystal structures exist of the archaeal aspartate transporter  $\text{Glt}_{\text{Ph}}$  homolog, an established model system for EAATs [75–77]. For instance, substrate transport is achieved by a large elevator-like transition from an outward- to an inward-facing conformation, which moves the bound transmitter from one side of the membrane to the other (Fig. 9A). However, these crystal structures do not provide any information on the location of the anion channel and the anion-conducting conformation of the transporter.

EAATs are homotrimers with each monomer constituting a fully functional transporter and channel. In patch-clamp or two-electrode voltage clamp experiments, two distinct current components can be reliably distinguished: thermodynamically uncoupled anion fluxes and electrogenic glutamate transport [78]. EAAT anion channels are activated by transport substrates such as  $\text{Na}^+$  and glutamate. Opening and closing of these channels is assumed to be tightly linked to transitions within the glutamate uptake cycle [79]. In recent years, several side chain mutations were identified that affect anion permeation properties such as unitary conductance or relative anion selectivities [80,81]. It was hypothesized that parts of the anion pore were dynamically formed during the glutamate transport cycle [82]. Thus, most mutations affect both channel and glutamate transport activities at the same time, and experimental structure–function investigations alone turned out to be insufficient to draw a conclusive picture of the EAAT anion channel.

CompEL MD simulations, however, were indeed able to resolve the mystery of the EAAT anion conductance [74]. At voltages from  $\pm 500$  mV to  $\pm 1.6$  V the available outward- and inward-facing  $\text{Glt}_{\text{Ph}}$  X-ray structures were non-conductive to ions on timescales of several microseconds (Fig. 9A). However, for certain intermediate conformations along the transition path from the outward- to the inward-facing  $\text{Glt}_{\text{Ph}}$  conformation, we observed a fully reversible transition to the transporter's *channel conformation*. Within hundreds of nanoseconds, lateral movement of the so-called transport domain created an anion-

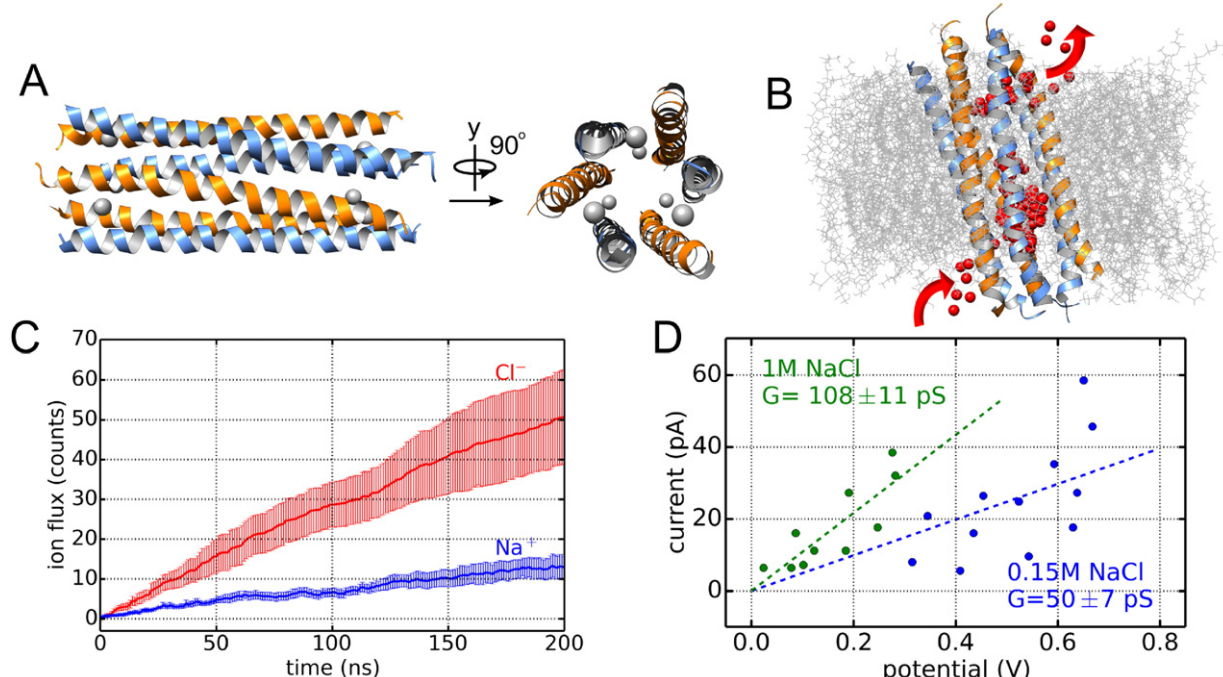


**Fig. 8.** Ion permeation across the dermcidin antimicrobial peptide. (A) Side and top view of the hexameric channel crystal structure. (B) The channel tilts when embedded in a lipid bilayer. Red spheres show the trajectory of a  $\text{Cl}^-$  ion during a complete permeation event. Other ions and water molecules are omitted for clarity. (C) Ion permeations of  $\text{Na}^+$  and  $\text{Cl}^-$  in 0.15 M NaCl. The solid line shows the average count obtained from six independent simulations; the error bars show the standard error. (D) I–V plots derived from 100 ns CompEL trajectories in 0.15 M and 1.0 M NaCl respectively. The slope of the linear fits (dashed lines) yields the average conductance. (Panel C appeared as Fig. S7B, panel D as Fig. 3D of Ref. [69].)

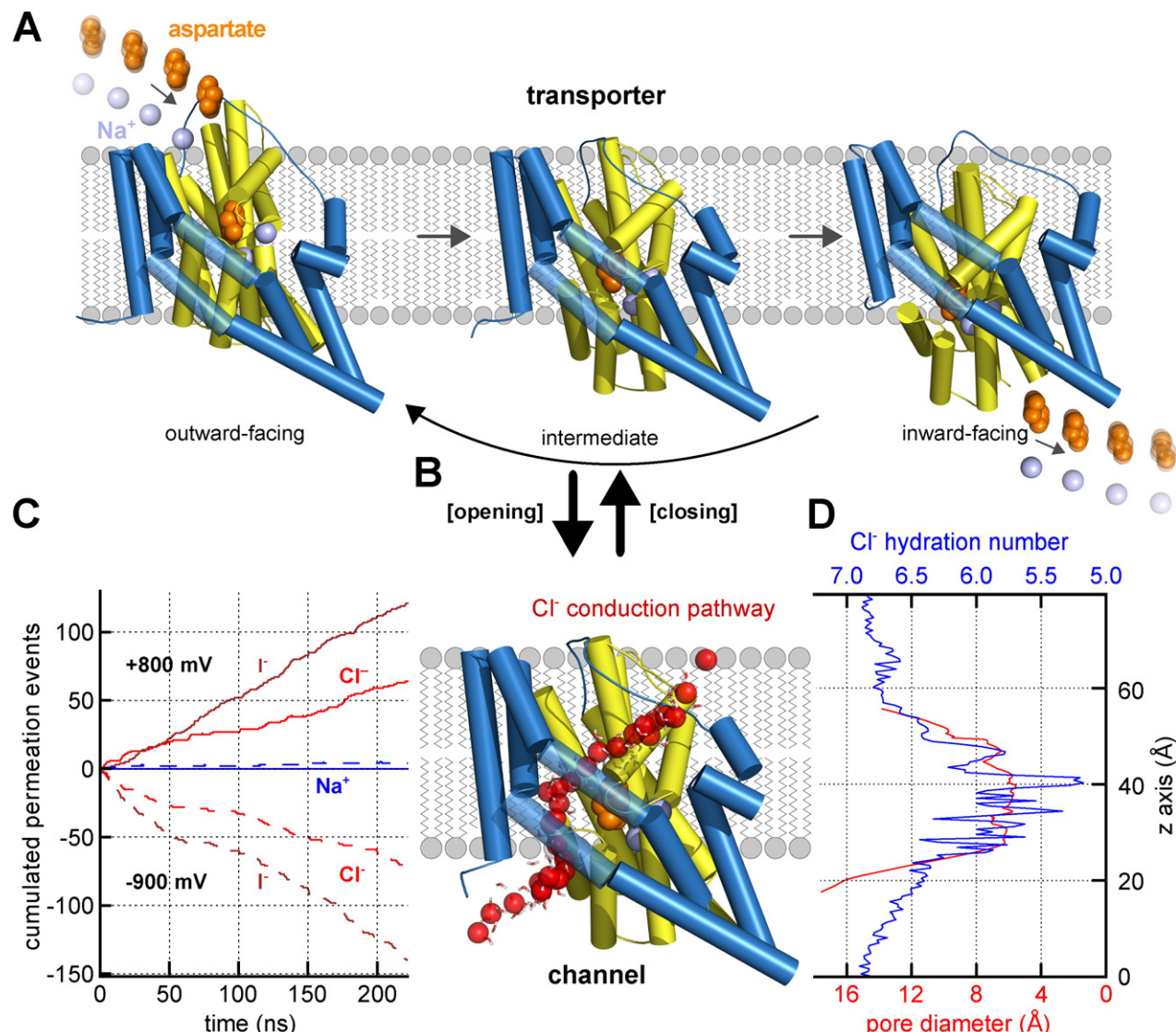


**Fig. 9.** Anion permeation through the glutamate transporter homolog Glt<sub>Ph</sub>. (A) Illustration of the glutamate/aspartate uptake cycle. For clarity, only one monomer of the Glt<sub>Ph</sub> trimer is depicted. The static trimerization domain is shown in blue cartoon representation, the mobile transport domain in yellow. The transport cycle involves substrate binding from the extracellular space to the outward-facing conformation (PDB 2NWX), transition through intermediate states [74] to the inward-facing conformation (PDB 3KBC), substrate dissociation and retranslocation. (B) Illustration of the Glt<sub>Ph</sub> anion channel-forming conformation. An anion pore along the interdomain interface is created via lateral movement of the transport domain in intermediate transport conformations. Red spheres represent a single permeating Cl<sup>-</sup> ion. (C) Cumulative permeation count from CompEL simulations of Glt<sub>Ph</sub> at +800 mV or -900 mV in the presence of 1 M NaCl or NaI. (D) Pore profile of anion hydration and pore diameter. Hydration numbers are integrals of Cl<sup>-</sup>/hydrogen radial distribution functions to the first minimum. Figure partially reprinted from Ref. [74] with permission from Elsevier.

selective pore, which was immediately filled with water (Fig. 9B). The following onset of anion permeation enabled the identification of the anion permeation pathway.

The simulations reproduced the experimentally determined anion selectivity [78]. Under simulation conditions, the observed Cl<sup>-</sup> conductances around 50 pS at  $\approx 800$  mV and 1 M NaCl are higher and not directly comparable to the experimental data which were obtained under more physiological conditions (Fig. 9C). In particular, experimental EAAT anion currents show nonlinear current–voltage relationships, which preclude a linear extrapolation of experimental data to the simulated voltages, or vice-versa [83,84]. However, using Eyring rate models derived from experimental I–V curves, the measurements were extrapolated to the simulation conditions and the CompEL results and experiments were found to be consistent. The model for the anion channel shows unique features distinct from other biological ion channels: in agreement with ion substitution experiments [78], the anion pore has a large diameter of  $\sim 5$  Å and anions permeate in a partially hydrated state (Fig. 9D). Furthermore, a single arginine was identified to be the

main determinant of the anion selectivity of these channels. To allow for further experimental testing of these findings, an exhaustive *in silico* screening of mutations of pore-lining residues was performed by using CompEL simulations. Several substitutions were identified that either increase or decrease anion currents. In patch-clamp experiments on homologous mutations inserted into mammalian EAATs, non-stationary noise analysis revealed effects comparable to the mutants identified in the simulations. Surprisingly, three mutants even converted the anion channel into a non-selective anion/cation channel (Fig. 10A). Consistently, the cation permeability observed in these simulations could be confirmed by reversal potential measurements (Fig. 10B).

The identification of the EAAT anion conduction mechanism would not have been possible without the use of molecular simulations. With CompEL, anion conduction by Glt<sub>Ph</sub> was directly simulated and key ion conduction properties, which were accessible to experiments (such as unitary conductance or anion/cation selectivity) could be readily determined from simulations. This gave rise to further experimental validation and informed a number of additional experiments, which

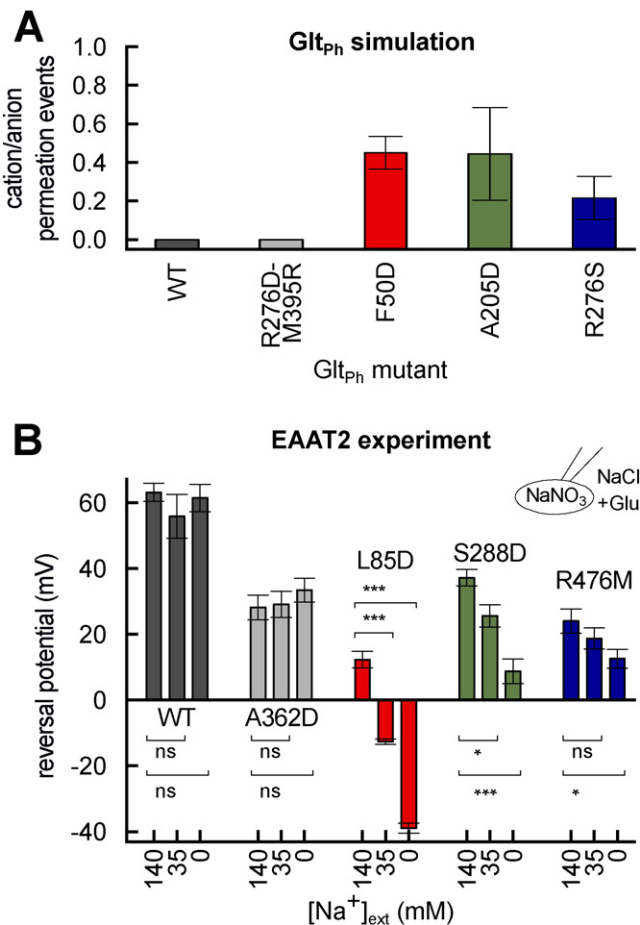


**Fig. 10.** Modification of ion selectivity in EAAT ion channels guided by CompEL. (A) CompEL simulations identified three Glt<sub>Ph</sub> mutants that convert the anion pore into a cation-conducting channel. Shown are cation/anion permeation ratios from the simulations of the wild-type, another anion-selective mutant and three variants with significant Na<sup>+</sup> permeability. (B) Experimental validation on homologous mutants of the human EAAT2 transporter, indicated by the same color as in (A), by whole-cell patch-clamp experiments. Side chain substitutions with prominent Na<sup>+</sup> currents in the simulations show significant alterations of the measured reversal potential upon changes in extracellular [Na<sup>+</sup>]. Reprinted from Ref. [74] with permission from Elsevier.

together were able to draw a comprehensive picture of the EAAT anion channel.

#### 4. Discussion

##### 4.1. Strengths and limitations of the position exchange protocol

In the original publication [34], two protocols to perform ion/water position exchanges were introduced: the *deterministic* and the *non-equilibrium switching* protocol. The deterministic protocol has a negligible impact on simulation performance, and the impact of the ion/water position exchanges on the propagation of the rest of the MD system was shown to be extremely small, see Fig. 2. A significant effect is observed for only about a dozen atoms in the direct vicinity of the exchanged molecules, see Fig. 5 in Ref. [34]. This is usually inconsequential since the molecules chosen for the exchanges are the ones farthest from the channels under consideration.

While in the deterministic protocol positions are swapped instantaneously, the non-equilibrium protocol performs short (e.g., 1 ps) transition simulations, in which a water molecule, for example in compartment A, and an ion in compartment B are smoothly transformed into one another with a  $\lambda$ -dependent Hamiltonian. The transition is accepted with a probability according to the Metropolis Monte Carlo

criterion, where the work associated with the transition appears in the exponential. An additional additive term in the exponential allows the user to set an energy difference between the compartments that effectively leads to a (possibly fractional) charge imbalance and thus a transmembrane potential difference between the compartments. The advantage of the non-equilibrium protocol is that on average, non-integer values of  $\Delta q$  can be established, so that small values of  $\Delta U$  are more easily effectuated. In contrast, the smallest value of  $\Delta U$  in the deterministic protocol depends on the MD system size and is limited by the smallest possible charge imbalance of  $\Delta q_{\min} = 2e^-$  arising from a difference of a single ionic charge between the compartments. For small MD systems, such as in our KcsA example, this can already give rise to a voltage difference of about 200 mV (Figs. 1C, D and 6).

The major disadvantage of the non-equilibrium protocol is that after a steady state between channel current and trans-compartment exchanges is reached, the fraction of accepted Monte Carlo moves becomes very small, which leads to the rejection of a substantial portion of the MD trajectory. Since the resulting channel currents and selectivities were shown to be identical for both protocols, the deterministic protocol is the one commonly adopted and all the results on ion channels covered by this review were based on using this protocol.

The ion/water exchange protocol is particularly efficient at determining conductances for large channels (e.g., in PorB). Yet, high ion currents through large pores may over time lead to a decrease in the number of water molecules in one compartment. This is a result of the solvation shell of the ions traveling with the ions through the pore. While ions are continuously swapped back into the other compartment, the solvation shell is not. At the same time, the osmotic effect, which would lead to water preferably flowing into the compartment with the higher ion concentration, is minor and thus too small to compensate for a slight depletion of water in one of the compartments. Although this problem arises only in high-conductance pores, defining position restraints on the channel centers and ensuring that the water compartments are sufficiently large may alleviate this problem.

It should be noted that sustained ionic flow through membrane channels can also be achieved using single membrane systems. The non-periodic energy step method [30] implemented for NAMD [85] is an example for this. An advantage of using a single membrane is a smaller MD system size. However, the duplication of membrane and channel common for CompEL also enhances sampling and enables investigation of positive and negative membrane voltages at the same time, and therefore the additionally invested computer time due to system size is usually put to good use.

##### 4.2. Voltage fluctuations in small systems

A high level of fluctuation in the membrane voltage is often thought to be an undesired and inherent consequence of ion/water positional exchanges in CompEL. We therefore investigated the level of fluctuation in double-bilayer systems *without* any exchanges of ion/water positions. The average transmembrane potential difference in double-membrane setups is a result of the charge imbalance  $\Delta q$  between the aqueous compartments. For the potential drop  $\Delta U$  across the membrane, only the charge distribution perpendicular to the membrane (typically in z direction) is relevant, so that  $\Delta U$  can be obtained by integrating twice over the charge distribution within bins along z (Fig. 1D). In contrast to single-cell electrophysiology with patch sizes on the order of  $\mu\text{m}^2$  and time resolutions of, minimally,  $\mu\text{s}$ , the patch sizes used in CompEL are typically orders of magnitude smaller, while in the dimension of time even instantaneous voltages can be calculated from snapshots of the configuration obtained at a particular time step. Our studies show that the fluctuations in  $\Delta U$  become larger both for shrinking patch sizes and for a decrease in the time span used for time averaging. We demonstrate here that the fluctuations are a “feature” of the small system size and simulation times, while they are unrelated to whether position

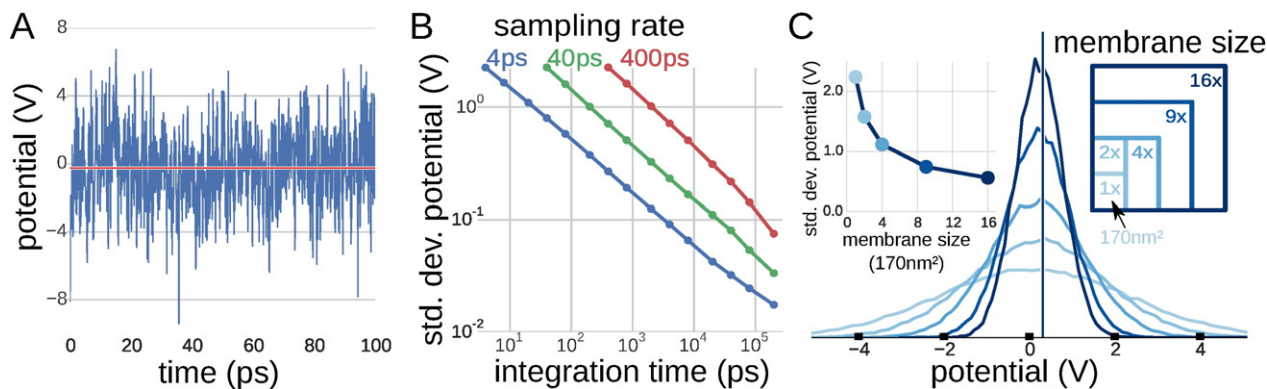


**Fig. 11.** Analysis of transmembrane potential fluctuations in double-membrane simulation setups without ion/water swaps. (A) The transmembrane potential  $\Delta U$  (blue) of a 170 nm<sup>2</sup> patch of POPC lipids shows fluctuations of several volts about the average (red) when calculated from instantaneous snapshots of the charge distribution. Here, a  $\Delta q = 2e^-$  charge imbalance was applied. (B) The size of the fluctuations decreases with longer averaging time windows. For uncorrelated recordings of the charge distribution, i.e., when the time between recordings is long compared to the auto-correlation time of  $\approx 0.2$  ps, the width of the potential distribution depends on how many instantaneous recordings are averaged. Panel (C) shows how the calculated instantaneous voltage fluctuations decrease with larger patch sizes. Here, patch size and charge imbalance were scaled by the same factor each, resulting in the same time-averaged transmembrane potential.

exchanges are performed and whether channels are present in the membranes.

Fig. 11A shows  $\Delta U(t) = U_B(t) - U_A(t)$ , calculated from individual time steps for a system with a membrane surface of 170 nm<sup>2</sup> at a charge difference of  $\Delta q = 2e^-$ . For  $U_A$  and  $U_B$ , the z-average over a water layer with a thickness of about 2.5 nm, centered around the midplane of the compartment, was used. The potential fluctuates by several volts about the average with a very short auto-correlation time of  $\approx 0.2$  ps. Note that no ion exchanges occur in this system and that the voltage difference is simply generated by a continuous ion imbalance. Compared to the noise typically encountered in patch clamp experiments and to physiological transmembrane voltages of <100 mV, these fluctuations appear very high. However, analogous to thermodynamic properties such as temperature and pressure which both also exhibit large fluctuations on the time and length scales of MD simulations, these fluctuations are expected given the short time scales and the small number of particles in the CompEL systems under these conditions.

The membrane voltage as measured in patch clamp experiments is a time average over, minimally, several microseconds. Fig. 11B shows how the time interval entering the average influences the standard deviation of the transmembrane voltage. We next investigated the effect of the number of frames saved in the output trajectory on the calculated level of the voltage fluctuations (blue, green and red lines in Fig. 11B). We conclude that, because in the current implementation the voltage is determined retrospectively, the observed voltage fluctuations chiefly result from retaining a limited number of configurations in the output trajectory. Fig. 11C, in addition, shows how an increase in the membrane patch area reduces the fluctuations in the calculated voltage. Therefore, both the recording of a high number of frames per time span and the use of a sufficiently large membrane patch help minimize the voltage fluctuation level in double-bilayer systems, which is a direct physical result of the limited simulation system size and not of the ion exchange protocol.

## Transparency Document

The Transparency document associated with this article can be found, in online version.

## Acknowledgments

This work was supported by the German Research Foundation (DFG) through the collaborative research center SFB803, project A03. Chen Song is supported by a Marie Curie intra-European fellowship

within the 7th European Community framework programme. Ulrich Zachariae acknowledges funding from the Scottish Universities' Physics Alliance. We thank Julian Tim Brennecke for helping with data reprocessing and Helmut Grubmüller for fruitful discussions.

## Appendix A. Supplementary data

Supplementary data to this article can be found online at <http://dx.doi.org/10.1016/j.bbamem.2016.02.006>.

## References

- [1] B. Hille, Ion Channels of Excitable Membranes, third ed. Sinauer, Sunderland, MA, 2001.
- [2] F.H. Epstein, M.J. Ackerman, D.E. Clapham, Ion channels – basic science and clinical disease, *N. Engl. J. Med.* 336 (22) (1997) 1575–1586.
- [3] J.-K. Zhu, Regulation of ion homeostasis under salt stress, *Curr. Opin. Plant Biol.* 6 (5) (2003) 441–445.
- [4] A. Verkhratsky, O.A. Krizhkal, O.H. Petersen, From Galvani to patch clamp: the development of electrophysiology, *Pflügers Arch.* 453 (3) (2006) 233–247.
- [5] F. Ashcroft, Ion Channels and Disease, Elsevier, 2000.
- [6] D.A. Doyle, J.M. Cabral, R.A. Pfuettner, A. Kuo, J.M. Gulbis, S.L. Cohen, B.T. Chait, R. MacKinnon, The structure of the potassium channel: molecular basis of K<sup>+</sup> conduction and selectivity, *Science* 280 (5360) (1998) 69–77.
- [7] Y. Zhou, J.H. Morais-Cabral, A. Kaufman, R. MacKinnon, Chemistry of ion coordination and hydration revealed by a K<sup>+</sup> channel–Fab complex at 2.0 Å resolution, *Nature* 414 (6859) (2001) 43–48.
- [8] R. Dutzler, E.B. Campbell, M. Cadene, B.T. Chait, R. MacKinnon, X-ray structure of a CIC chloride channel at 3.0 Å reveals the molecular basis of anion selectivity, *Nature* 415 (6869) (2002) 287–294.
- [9] J. Payandeh, T. Scheuer, N. Zheng, W.A. Catterall, The crystal structure of a voltage-gated sodium channel, *Nature* 475 (7356) (2011) 353–358.
- [10] X. Hou, L. Pedi, M.W. Diver, S.B. Long, Crystal structure of the calcium release-activated calcium channel Orai, *Science* 338 (6112) (2012) 1308–1313.
- [11] M.S. Weiss, U. Abele, J. Weckesser, W. Welte, E. Schiltz, G.E. Schulz, Molecular architecture and electrostatic properties of a bacterial porin, *Science* 254 (5038) (1991) 1627–1630.
- [12] S.W. Cowan, T. Schirmer, G. Rummel, M. Steiert, R. Ghosh, R.A. Paupert, J.N. Jansoni, J.P. Rosenbusch, Crystal structures explain functional properties of two *E. coli* porins, *Nature* 358 (6389) (1992) 727–733.
- [13] S. Bernèche, B. Roux, A microscopic view of ion conduction through the K<sup>+</sup> channel, *PNAS* 100 (15) (2003) 8644–8648.
- [14] S.Y. Noskov, S. Bernèche, B. Roux, Control of ion selectivity in potassium channels by electrostatic and dynamic properties of carbonyl ligands, *Nature* 431 (7010) (2004) 830–834.
- [15] M.O. Jensen, D.W. Borhani, K. Lindorff-Larsen, P. Maragakis, V. Jogini, M.P. Eastwood, R.O. Dror, D.E. Shaw, Principles of conduction and hydrophobic gating in K<sup>+</sup> channels, *PNAS* 107 (13) (2010) 5833–5838.
- [16] M.O. Jensen, V. Jogini, D.W. Borhani, A.E. Leffler, R.O. Dror, D.E. Shaw, Mechanism of voltage gating in potassium channels, *Science* 336 (6078) (2012) 229–233.
- [17] C. Maffeo, S. Bhattacharya, J. Yoo, D. Wells, A. Aksimentiev, Modeling and simulation of ion channels, *Chem. Rev.* 112 (12) (2012) 6250–6284.
- [18] A.D. Mackerell, Empirical force fields for biological macromolecules: overview and issues, *J. Comput. Chem.* 25 (13) (2004) 1584–1604.

- [19] J.L. Klepeis, K. Lindorff-Larsen, R.O. Dror, D.E. Shaw, Long-timescale molecular dynamics simulations of protein structure and function, *Curr. Opin. Struct. Biol.* 19 (2) (2009) 120–127.
- [20] Q. Zhong, P.B. Moore, D.M. Newns, M.L. Klein, Molecular dynamics study of the LS3 voltage-gated ion channel, *FEBS Lett.* 427 (2) (1998) 267–270.
- [21] A. Suenaga, Y. Komeiji, M. Uebayasi, T. Meguro, M. Saito, I. Yamato, Computational observation of an ion permeation through a channel protein, *Biosci. Rep.* 18 (1998) 39–48.
- [22] D.P. Tieleman, H.J.C. Berendsen, M.S.P. Sansom, Voltage-dependent insertion of alamethicin at phospholipid/water and octane/water interfaces, *Biophys. J.* 80 (1) (2001) 331–346.
- [23] P.S. Crozier, D. Henderson, R.L. Rowley, D.D. Busath, Model channel ion currents in NaCl<sup>−</sup> extended simple point charge water solution with applied-field molecular dynamics, *Biophys. J.* 81 (6) (2001) 3077–3089.
- [24] A. Aksimentiev, K. Schulten, Imaging α-hemolysin with molecular dynamics: ionic conductance, osmotic permeability, and the electrostatic potential map, *Biophys. J.* 88 (6) (2005) 3745–3761.
- [25] B. Roux, The membrane potential and its representation by a constant electric field in computer simulations, *Biophys. J.* 95 (9) (2008) 4205–4216.
- [26] J. Gumbart, F. Khalili-Araghi, M. Sotomayor, B. Roux, Constant electric field simulations of the membrane potential illustrated with simple systems, *Biochim. Biophys. Acta Biomembr.* 1818 (2) (2012) 294–302.
- [27] L. Delemotte, F. Dehez, W. Treptow, M. Tarek, Modeling membranes under a transmembrane potential, *J. Phys. Chem. B* 112 (18) (2008) 5547–5550.
- [28] W. Treptow, M. Tarek, M.L. Klein, Initial response of the potassium channel voltage sensor to a transmembrane potential, *J. Am. Chem. Soc.* 131 (6) (2009) 2107–2109.
- [29] L. Delemotte, M. Tarek, M.L. Klein, C. Amaral, W. Treptow, Intermediate states of the Kv1.2 voltage sensor from atomistic molecular dynamics simulations, *PNAS* 108 (15) (2011) 6109–6114.
- [30] F. Khalili-Araghi, B. Zervogel, J.C. Gumbart, B. Roux, Molecular dynamics simulations of membrane proteins under asymmetric ionic concentrations, *J. Gen. Physiol.* 142 (4) (2013) 465–475.
- [31] B. Roux, The calculation of the potential of mean force using computer simulations, *Comput. Phys. Commun.* 91 (1) (1995) 275–282.
- [32] S. Bernèche, B. Roux, Energetics of ion conduction through the K<sup>+</sup> channel, *Nature* 414 (6859) (2001) 73–77.
- [33] Y. Liu, F. Zhu, Collective diffusion model for ion conduction through microscopic channels, *Biophys. J.* 104 (2) (2013) 368–376.
- [34] C. Kutzner, H. Grubmüller, B.L. de Groot, U. Zachariae, Computational electrophysiology: the molecular dynamics of ion channel permeation and selectivity in atomistic detail, *Biophys. J.* 101 (2011) 809–817.
- [35] J.N. Sachs, P.S. Crozier, T.B. Woolf, Atomistic simulations of biologically realistic transmembrane potential gradients, *J. Chem. Phys.* 121 (22) (2004) 10847–10851.
- [36] A.A. Gurtovenko, I. Vattulainen, Pore formation coupled to ion transport through lipid membranes as induced by transmembrane ionic charge imbalance: atomistic molecular dynamics study, *J. Am. Chem. Soc.* 127 (50) (2005) 17570–17571.
- [37] B. Roux, Influence of the membrane potential on the free energy of an intrinsic protein, *Biophys. J.* 73 (6) (1997) 2980.
- [38] D.A. Köpfer, C. Song, T. Gruene, G.M. Sheldrick, U. Zachariae, B.L. de Groot, Ion permeation in K<sup>+</sup> channels occurs by direct Coulomb knock-on, *Science* 346 (6207) (2014) 352–355.
- [39] J.S. Hub, B.L. de Groot, H. Grubmüller, G. Groenhof, Quantifying artifacts in Ewald simulations of inhomogeneous systems with a net charge, *J. Chem. Theory Comput.* 10 (1) (2014) 381–390.
- [40] S. Páll, M.J. Abraham, C. Kutzner, B. Hess, E. Lindahl, Tackling exascale software challenges in molecular dynamics simulations with GROMACS, in: S. Markidis, E. Laure (Eds.), *Lecture Notes in Computer Science 8759, EASC 2014*, Springer International Publishing, Switzerland 2015, pp. 1–25.
- [41] M.J. Abraham, T. Murtola, R. Schulz, S. Páll, J.C. Smith, B. Hess, E. Lindahl, GROMACS: high performance molecular simulations through multi-level parallelism from laptops to supercomputers, *SoftwareX* 1–2 (2015) 19–25.
- [42] M.J. Abraham, D. van der Spoel, E. Lindahl, B. Hess, The GROMACS Development Team, *GROMACS User Manual Version 5.1*, 2015.
- [43] K. Zeth, K. Diederichs, W. Welte, H. Engelhardt, Crystal structure of Omp32, the anion-selective porin from *Comamonas acidovorans*, in complex with a periplasmic peptide at 2.1 Å resolution, *Structure* 8 (9) (2000) 981–992.
- [44] W. Im, B. Roux, Ion permeation and selectivity of OmpF porin: a theoretical study based on molecular dynamics, Brownian dynamics, and continuum electrodiffusion theory, *J. Mol. Biol.* 322 (4) (2002) 851–869.
- [45] U. Zachariae, V. Helms, H. Engelhardt, Multistep mechanism of chloride translocation in a strongly anion-selective porin channel, *Biophys. J.* 85 (2) (2003) 954–962.
- [46] K. Zeth, M. Thein, Porins in prokaryotes and eukaryotes: common themes and variations, *Biochem. J.* 431 (2010) 13–22.
- [47] K. Zeth, Structure and evolution of mitochondrial outer membrane proteins of β-barrel topology, *Biochim. Biophys. Acta Bioenerg.* 1797 (6) (2010) 1292–1299.
- [48] J.-M. Pagès, C.E. James, M. Winterhalter, The porin and the permeating antibiotic: a selective diffusion barrier in Gram-negative bacteria, *Nat. Rev. Microbiol.* 6 (12) (2008) 893–903.
- [49] H. Nikaido, Molecular basis of bacterial outer membrane permeability revisited, *Microbiol. Mol. Biol. Rev.* 67 (4) (2003) 593–656.
- [50] M. Tanabe, C.M. Nimigean, T.M. Iverson, Structural basis for solute transport, nucleotide regulation, and immunological recognition of *Neisseria meningitidis* PorB, *PNAS* 107 (15) (2010) 6811–6816.
- [51] C. Kattner, D.N. Toussi, J. Zaucha, L.M. Wetzel, N. Rüppel, U. Zachariae, P. Massari, M. Tanabe, Crystallographic analysis of *Neisseria meningitidis* PorB extracellular loops potentially implicated in TLR2 recognition, *J. Struct. Biol.* 185 (3) (2014) 440–447.
- [52] M. Olesky, S. Zhao, R.L. Rosenberg, R.A. Nicholas, Porin-mediated antibiotic resistance in *Neisseria gonorrhoeae*: ion, solute, and antibiotic permeation through PIB proteins with penB mutations, *J. Bacteriol.* 188 (7) (2006) 2300–2308.
- [53] G. Bainbridge, I. Gokce, J.H. Lakey, Voltage gating is a fundamental feature of porin and toxin β-barrel membrane channels, *FEBS Lett.* 431 (3) (1998) 305–308.
- [54] D.J. Müller, A. Engel, Voltage and pH-induced channel closure of porin OmpF visualized by atomic force microscopy, *J. Mol. Biol.* 285 (4) (1999) 1347–1351.
- [55] R. Koebnik, K.P. Locher, P. Van Gelder, Structure and function of bacterial outer membrane proteins: barrels in a nutshell, *Mol. Microbiol.* 37 (2) (2000) 239–253.
- [56] A.C. Le Dain, C.C. Häse, J. Tommassen, B. Martinac, Porins of *Escherichia coli*: unidirectional gating by pressure, *EMBO J.* 15 (14) (1996) 3524.
- [57] M. Colombini, VDAC structure, selectivity, and dynamics, *Biochim. Biophys. Acta Biomembr.* 1818 (6) (2012) 1457–1465.
- [58] V. Shoshan-Barmatz, D. Ben-Hail, VDAC, a multi-functional mitochondrial protein as a pharmacological target, *Mitochondrion* 12 (1) (2012) 24–34.
- [59] U. Zachariae, R. Schneider, R. Briones, Z. Gattin, J.-P. Demers, K. Giller, E. Maier, M. Zweckstetter, C. Griesinger, S. Becker, et al., β-barrel mobility underlies closure of the voltage-dependent anion channel, *Structure* 20 (9) (2012) 1540–1549.
- [60] P.S. Phale, T. Schirmer, A. Prilipov, K.-L. Lou, A. Hardtmeyer, J.P. Rosenbusch, Voltage gating of *Escherichia coli* porin channels: role of the constriction loop, *PNAS* 94 (13) (1997) 6741–6745.
- [61] W. Grosse, G. Psakis, B. Mertins, P. Reiss, D. Windisch, F. Brademann, J. Bürck, A. Ulrich, U. Koert, L.-O. Essen, Structure-based engineering of a minimal porin reveals loop-independent channel closure, *Biochemistry* 53 (29) (2014) 4826–4838.
- [62] A.J. Wolfe, M.M. Mohammad, A.K. Thakur, L. Movileanu, Global redesign of a native β-barrel scaffold, *Biochim. Biophys. Acta Biomembr.* 1858 (2016) 19–29.
- [63] C. Miller, See potassium run, *Nature* 414 (6859) (2001) 23–24.
- [64] Y. Zhou, R. MacKinnon, The occupancy of ions in the K<sup>+</sup> selectivity filter, *J. Mol. Biol.* 333 (5) (2003) 965–975.
- [65] M. LeMasurier, L. Heginbotham, C. Miller, KcsA it's a potassium channel, *J. Gen. Physiol.* 118 (3) (2001) 303–314.
- [66] C.B. Hübschle, G.M. Sheldrick, B. Dittrich, ShelXle: a Qt graphical user interface for SHEXL, *J. Appl. Crystallogr.* 44 (6) (2011) 1281–1284.
- [67] G.M. Sheldrick, A short history of SHEXL, *Acta Crystallogr., Sect. A: Found. Crystallogr.* 64 (1) (2007) 112–122.
- [68] R.E.W. Hancock, H.-G. Sahl, Antimicrobial and host-defense peptides as new anti-infective therapeutic strategies, *Nat. Biotechnol.* 24 (12) (2006) 1551–1557.
- [69] C. Song, C. Weichbrodt, E. Salnikov, M. Dynowski, B. Forsberg, B. Bechinger, C. Steinem, B.L. de Groot, U. Zachariae, K. Zeth, Crystal structure and functional mechanism of a human antimicrobial membrane channel, *PNAS* 110 (2013) 4586–4591.
- [70] N. Zerangue, M.P. Kavanaugh, Flux coupling in a neuronal glutamate transporter, *Nature* 383 (6601) (1996) 634–637.
- [71] W.A. Fairman, R.J. Vandenberg, J.L. Arriza, M.P. Kavanaugh, S.G. Amara, An excitatory amino-acid transporter with properties of a ligand-gated chloride channel, *Nature* 375 (6532) (1995) 599–603.
- [72] S.A. Picaud, H.P. Larsson, G.B. Grant, H. Lecar, F.S. Werblin, Glutamate-gated chloride channel with glutamate-transporter-like properties in cone photoreceptors of the tiger salamander, *J. Neurophysiol.* 74 (4) (1995) 1760–1771.
- [73] N. Winter, P. Kovermann, C. Fahlke, A point mutation associated with episodic ataxia 6 increases glutamate transporter anion currents, *Brain* 135 (Pt 11) (2012) 3416–3425.
- [74] J.P. Machtens, D. Kortzak, C. Lansche, A. Leinenweber, P. Kilian, B. Begemann, U. Zachariae, D. Ewers, B.L. de Groot, R. Briones, C. Fahlke, Mechanisms of anion conduction by coupled glutamate transporters, *Cell* 160 (3) (2015) 542–553.
- [75] O. Boudker, R.M. Ryan, D. Yernool, K. Shimamoto, E. Gouaux, Coupling substrate and ion binding to extracellular gate of a sodium-dependent aspartate transporter, *Nature* 445 (7126) (2007) 387–393.
- [76] N. Reyes, C. Ginter, O. Boudker, Transport mechanism of a bacterial homologue of glutamate transporters, *Nature* 462 (7275) (2009) 880–885.
- [77] S. Jensen, A. Guskov, S. Rempel, I. Hanelt, D.J. Slotboom, Crystal structure of a substrate-free aspartate transporter, *Nat. Struct. Mol. Biol.* 20 (10) (2013) 1224–1226.
- [78] J.I. Wadiche, M.P. Kavanaugh, Macroscopic and microscopic properties of a cloned glutamate transporter/chloride channel, *J. Neurosci.* 18 (19) (1998) 7650–7661.
- [79] J.P. Machtens, P. Kovermann, C. Fahlke, Substrate-dependent gating of anion channels associated with excitatory amino acid transporter 4, *J. Biol. Chem.* 286 (27) (2011) 23780–23788.
- [80] R.M. Ryan, A.D. Mitrovic, R.J. Vandenberg, The chloride permeation pathway of a glutamate transporter and its proximity to the glutamate translocation pathway, *J. Biol. Chem.* 279 (20) (2004) 20742–20751.
- [81] P. Kovermann, J.P. Machtens, D. Ewers, C. Fahlke, A conserved aspartate determines pore properties of anion channels associated with excitatory amino acid transporter 4, *J. Biol. Chem.* 285 (31) (2010) 23676–23686.
- [82] R.J. Cater, R.J. Vandenberg, R.M. Ryan, The domain interface of the human glutamate transporter EAAT1 mediates chloride permeation, *Biophys. J.* 107 (3) (2014) 621–629.
- [83] N. Melzer, A. Biela, C. Fahlke, Glutamate modifies ion conduction and voltage-dependent gating of excitatory amino acid transporter-associated anion channels, *J. Biol. Chem.* 278 (50) (2003) 50112–50119.
- [84] C. Fahlke, D. Kortzak, J.P. Machtens, Molecular physiology of EAAT anion channels, *Pflugers Arch. - Eur. J. Physiol.* 468 (3) (2016) 491–502.
- [85] J.C. Phillips, R. Braun, W. Wang, J. Gumbart, E. Tajkhorshid, E. Villa, C. Chipot, R.D. Skeel, L. Kale, K. Schulten, Scalable molecular dynamics with NAMD, *J. Comput. Chem.* 26 (16) (2005) 1781–1802.